BNL-25484
AMD 810

CONF-790402--1

APPLICATIONS OF THE THERMIT CODE TO 3D THERMAL HYDRAULIC ANALYSIS OF LWR CORES*

William H. Reed
P.O. Box 380
Sylvania, Georgia 30467

H. Bruce Stewart
Applied Mathematics Department
Brookhaven National Laboratory
Upton, New York 11973

Lothar Wolf
Department of Nuclear Engineering
Massachusetts Institute of Technology
Cambridge, Massachusetts 02139

The THERMIT code calculates the three-dimensional transient thermal hydraulic behavior of light water reactor cores. Its two-fluid dynamics equations for two-phase flow offer improved physical modelling capability needed in the context of calculation coupled to neutron kinetics for feedback. The numerical fluid dynamics method was chosen for reliability over a wider range of transients. An improved heat transfer numerical method is presented which gives better numerical stability and accuracy. A number of example calculations are discussed which give an idea of the power and flexibility of the code.

*This work was supported in part by the Electric Power Research Institute and partially at Brookhaven National Laboratory under the auspices of the Department of Energy.

APPLICATIONS OF THE THERMIT CODE TO 3D THERMAL HYDRAULIC ANALYSIS OF LWR CORES

INTRODUCTION

Better understanding of the safety-related behavior of light water reactors (LWRs) will require continual upgrading of physical modelling, together with new and better numerical techniques. The THERMIT code offers advances on both planes in the area of thermal hydraulic analysis of LWR cores. THERMIT solves transient compressible fluid flow equations for both single-phase and two-phase flow in the rectangular geometry of the reactor core, simultaneously coupled with a fuel rod heat conduction model via a best estimate heat transfer package. The code was intended to analyze core-wide thermal hydraulic behavior during space-dependent transients using fluid flow control volumes whose transverse dimensions are roughly the size of an assembly.

In order to achieve a general multidimensional flow capability, we held two considerations uppermost. First, the code should solve the full multidimensional conservation equations. Some codes in the past have neglected certain terms in the transverse momentum equations, and while such approximations might be possible in special casses, their validity is hard to predict. Second, the numerical solution technique should not rely on any assumptions about the direction of flow. Codes such as COBRA-IIIC use a marching solution technique which solves the flow equations in finite difference form by marching one axial level at a time from inlet to outlet. Such techniques were natural for steady-state analysis, and can work satisfactorily for transients having sustained positive axial flow. However, they may work poorly for low axial flow or flow blockages, and not at all for even locally reversed flow.

A third criterion was also deemed important in the choice of a numerical approach: the method should be both reliable and efficient for a wide range of flow conditions. The best way to insure this is to choose a method whose convergence and stability properties have a sound mathematical basis.

These three criteria led us to select a semi-implicit finite difference method for the fluid dynamics based on the three-dimensional pressure field solution scheme developed for the TRAC code[1,2]. This method has a thorough mathematical grounding, which we shall briefly review below.

The THERMIT code accounts for heat transfer from one average fuel rod for each fluid control volume. The radial heat conduction equation in the rod is coupled to the fluid dynamics equations via a best estimate heat transfer package which determines the heat flux to the coolant. This heat flux is typically expressed as a coefficient h times a temperature difference. THERMIT uses a newly developed numerical method for calculating this heat flux as

$$\dot{q}'' = h^n(T_w^{n+1} - T_f^{n+1}),$$

where h is computed at the old time level n, but both the wall and fluid temperatures are taken at the new time level n+1. This doubly implicit numerical heat transfer coupling, which will be explained in more detail below, offers superior stability and accuracy, as will be shown in examples at the end of this paper.

The THERMIT code includes some physical models which are new to LWR core flow analysis. One is the method of calculating interbundle crossflow which results from our inistence on complete multidimensional momentum equations. With these equations the crossflow is determined by the net effect of pressure gradients, inertia (represented through the full set of multidimensional momentum convection terms), and friction laws describing resistance to transverse flow through tube banks. Comparison of this and an earlier model with experimental data are discussed below.

The primary application for which THERMIT was developed is eventual inclusion in a transient multidimensional reactor kinetics code with thermal hydraulic feedback. Because of the sensitivity of feedback to moderator density, the thermal dydraulics portion of such a code would need better physical modeling of coolant flow (especially as affects coolant void fraction) than previous models such as the homogeneous equilibrium model of two-phase flow (which was adequate when only critical heat flux ratios were required). This led us to choose a two-fluid model for two-phase flow in THERMIT. This model is based on six equations for the conservation of mass, momentum, and energy of each phase, with terms describing the interfacial exchanges between phases. THERMIT currently has preliminary models for momentum exchange and for phase change in the subcooled and nucleate boiling regions. These physically based models should have a wider range of validity than previous models, particularly for rapid transients.

Although THERMIT was developed for LWR core analysis with assembly-sized control volumes, another very important potential application of the code is subchannel analysis. The two-fluid model could be particularly useful for refill, reflood, and time-dependent blockage analysis. Initial tests have shown that THERMIT can compute equally well with subchannel control volumes, and future development in this area is planned.

The body of this paper has three parts. In the first, we review the basic ideas of the fluid dynamics method adapted from the TRAC code. Next we present our new, doubly implicit numerical method for treating heat transfer coupling between the fuel rod and coolant. These two parts are followed by a number of example calculations which demonstrate some of the capabilities of the code.

FLUID DYNAMICS METHOD

Before discussing the fluid dynamics calculation method, let us set down the partial differential equations of our two-fluid model of two-phase flow. These consist of conservation equations for mass, momentum, and energy of each

phase, with interfacial exchange terms Γ, F_i, and Q_i respectively:

$$\frac{\partial \alpha \rho_v}{\partial t} + \nabla \cdot (\alpha \rho_v \vec{v}_v) = \Gamma \tag{1a}$$

$$\frac{\partial (1-\alpha) \rho_\ell}{\partial t} + \nabla \cdot [(1-\alpha) \rho_\ell \vec{v}_\ell] = -\Gamma \tag{1b}$$

$$\frac{\partial \alpha \rho_v \vec{v}_v}{\partial t} + \nabla \cdot (\alpha \rho_v \vec{v}_v \vec{v}_v) + \alpha \nabla P = -\vec{F}_{wv} - \vec{F}_i - \alpha \rho_v \vec{g} \tag{1c}$$

$$\frac{\partial (1-\alpha) \rho_\ell \vec{v}_\ell}{\partial t} + \nabla \cdot [(1-\alpha) \rho_\ell \vec{v}_\ell \vec{v}_\ell] + (1-\alpha) \nabla P = -\vec{F}_{w\ell} + \vec{F}_i - (1-\alpha) \rho_\ell \vec{g} \tag{1d}$$

$$\frac{\partial \alpha \rho_v e_v}{\partial t} + \nabla \cdot (\alpha \rho_v e_v \vec{v}_v) + P \nabla \cdot (\alpha \vec{v}_v) + P \frac{\partial \alpha}{\partial t} = Q_{wv} + Q_i \tag{1e}$$

$$\frac{\partial (1-\alpha) \rho_\ell e_\ell}{\partial t} + \nabla \cdot [(1-\alpha) \rho_\ell e_\ell \vec{v}_\ell] + P \nabla \cdot [(1-\alpha) \vec{v}_\ell] - P \frac{\partial \alpha}{\partial t} = Q_{w\ell} - Q_i \tag{1f}$$

Since the momentum equations are vector equations, this makes a nonlinear system of 10 scalar partial differential equations. After specifying the exchange and source terms on the right hand sides, and furnishing microscopic equations of state for the density ρ and specific energy e of each phase, we have as unknowns the void fraction α, the pressure P, the phase temperatures T_v and T_ℓ, and the six components of the vapor and liquid velocities $\vec{v}_v$ and $\vec{v}_\ell$ for a total of ten unknowns. This two-fluid model is further discussed in references 2 through 6. The energy source terms will be described in the following section.

THERMIT may be applied to solve these equations in finite difference form for a wide range of thermal hydraulic transients. For very rapid transients, small time steps may be necessary; on the other hand, for slower transients larger time steps would be computationally more efficient. THERMIT is able to compute over a wide range of time step sizes. Not all transient codes can do this; for example, the COBRA-IIIC marching solution method [7] adapted from steady-state analysis may fail when very small time steps are tried. In this sense COBRA-IIIC is not truly a transient code.

Upper limits on time step size are typically associated with numerical stability questions. Physical phenomena have associated characteristic times, often related to spatial mesh size; to take Δt larger than such a characteristic time, the corresponding terms must be differenced implicitly. This introduces more terms into the equations to be solved for each time step. Sometimes a numerical method is said to use implicit differencing, but the solution procedure at each time step fails to account for all the coupling among unknowns. This may result in instability, or in a stable scheme which is very inefficient.

The numerical method in THERMIT treats as many terms implicitly as can be efficeintly accounted for in the solution procedure. The physical phenomena in equations 1 can be grouped as sonic propagation, interfacial exchanges, and fluid convection. In typical THERMIT applications, the first two have very short characteristic times and must be treated implicitly to allow Δt greater than a fraction of a millisecond. On the other hand, the time scale for fluid convection in a typical LWR core flow problem might be on the order of a tenth of a second. Therefore fluid convection is treated explicitly in the THERMIT difference equations. It is fortunate that the resulting limit $\Delta t < \Delta z/v$ (where v is a fluid velocity) is acceptable for a large number of THERMIT applications, since no fully implicit multidimensional multifluid calculation technique currently exists.

Let us now explain the method briefly; for more details, see references 3 and 8. The finite difference equations are written on a staggered mesh, wherein fluid properties such as α, P, T_v, T_ℓ, densities, and energies are defined at the center of each rectangular mesh cell, while each velocity component is defined at a different location, on the cell faces normal to that component. We will consider two dimensions for simplicity, denoting the cell center by (i,j). Velocities in the x direction are then defined at $(i\pm\frac{1}{2}, j)$, velocities in the y direction at $(i, j\pm\frac{1}{2})$. We shall suppress indices i and j themselves in writing difference equations, so that $\alpha_{i+\frac{1}{2}}$ refers to $(i+\frac{1}{2}, j)$; we also omit superscript n.

The vapor mass difference quation is

$$\alpha^{n+1}\rho_v^{n+1} - \alpha\rho_v + \frac{\Delta t}{\Delta x}\left[(\alpha\rho_v v_v^{x,n+1})_{i+\frac{1}{2}} - (\alpha\rho_v v_v^{x,n+1})_{i+\frac{1}{2}}\right]$$

$$+ \frac{\Delta t}{\Delta y}\left[(\alpha\rho_v v_v^{y,n+1})_{j+\frac{1}{2}} - (\alpha\rho_v v_v^{y,n+1})_{j-\frac{1}{2}}\right] = \Gamma^{n+\frac{1}{2}}$$

The phase change rate $\Gamma^{n+\frac{1}{2}}$ may be given by any expression involving smooth dependence on α, P, T_v, and T_ℓ at new time level n+1 in cell (i,j), as well as arbitrary dependence on old time level variables. Time levels chosen for the divergence terms reflect the goals set forth above: spatial differences of $\alpha\rho_v$ relate to convection[3] and are treated explicitly, while velocity gradients play a role in sonic propagation so the velocities must be at the new time. To maintain stability with explicity differenced convection, we use donor-cell rules for the determination of α and ρ_v at $(i\pm\frac{1}{2}, j)$ and $(i, j\pm\frac{1}{2})$ in the divergence terms, plus the requirement that

$$\Delta t < v_v^x/\Delta x, \quad \Delta t < v_v^y/\Delta y.$$

The liquid mass equation is differenced in a precisely analogous manner. The two energy equations are also quite similar; the additional velocity gradient term proportional to P is differenced with P and α at the old time and the velocities at the new time. The structure of all four equations is the same: each involves new time values of α, P, T_v, T_ℓ at the cell center and of the velocities on all faces. All other variables (e.g. neighboring α, P, T_v, T_ℓ) occur only at the old time level, and so will not enter as unknowns in the equations to be solved for each time step.

Next we consider the momentum equations. We use a non-conserative form of momentum equation derived from equation 1c, for example, by subtracting $\vec{v}_v$ times equation 1a from it. As an example, the resulting x direction momentum difference equation is

$$(\alpha\rho_v)_{i+\frac{1}{2}}(v_v^{x,n+1}-v_v^x)_{i+\frac{1}{2}} + \frac{\Delta t}{\Delta x}(\alpha\rho_v v_v^x)_{i+\frac{1}{2}}(\Delta_x v_v^x)_{i+\frac{1}{2}} + \frac{\Delta t}{\Delta y}(\alpha\rho_v v_v^y)_{i+\frac{1}{2}}(\Delta_y v_v^x)_{i+\frac{1}{2}} \quad (3)$$

$$+ \frac{\Delta t}{\Delta x}\alpha_{i+\frac{1}{2}}(P_{i+1}^{n+1} - P_i^{n+1}) = -(F_{iv}^x)_{i+\frac{1}{2}}^{n+\frac{1}{2}} - (F_{wv}^x)_{i+\frac{1}{2}}^{n+\frac{1}{2}}$$

Unlike the mass and energy equations, each momentum difference equation is spatially centered around a velocity point, in this case $(i+\frac{1}{2},j)$. Exchange and source terms in the x direction may depend on new time x direction velocities at $(i+\frac{1}{2},j)$; all other dependencies are permitted at the old time level only. Of course the pressure gradient term in equation 3 is intimately involved in sonic propagation, and the pressures there must be at the new time level in keeping with our stated goals. The velocity gradient terms represent momentum convection; they are differenced explicitly and using donor cell rules to define the velocity differences. Because the momentum convection terms are explicit, the structure of equation 3 in terms of new time unknowns is very simple: it involves vapor and liquid velocities at a single cell face $(i+\frac{1}{2},j)$ and the pressures at (i,j) and $(i+1,j)$ on either side. Similar structure is obtained for the liquid momentum equation, and for the two momentum equations in the y direction.

The procedure for solving the nonlinear difference equations at each time step is by Newton iteration. If the index m stands for Newton iteration number, and we denote the system of difference equations for a given time step by $F(x)=0$, where x stands for the new time level unknowns at all mesh points, we linearize and solve

$$F(x) \simeq F(x^{m+1}) = F(x^m) + J(x^m)(x^{m+1}-x^m) = 0$$

where J is the Jacobian matrix of F.

The linearized equations for each Newton iteration inherit the structure of the nonlinear difference equations: The four cell-centered equations for mass and energy involve only the unknowns P, α, T_v, T_ℓ in one cell, and the four surrounding velocities; while each momentum equation involves the vapor and liquid velocities at one cell face and the pressure on either side. A highly efficient solution technique exploits this structure as follows. First we reduce the two momentum equations at each cell face so that each involves the velocity of only one phase. Then we can easily eliminate velocities from the four cell-centered equations in favor of pressures in the cell and its immediate neighbors. We then have four linear equations invloving α, P, T_v, T_ℓ in cell (i,j), and P in surrounding cells. Finally we combine these to obtain one equation for P in cell (i,j) and its immediate neighbors.

The result of these operations is a system of linear equations for the pressures only. It turns out that these equations are of a very familiar type: in two dimensions they have a five stripe diagonally dominant coefficient matrix just like an elliptic difference problem. It can be shown in several simple cases[3] that the amount of diagonal dominance is $(h/c\Delta t)^2$, where h is mesh spacing

and c is some identifiable sonic velocity. This simple Poisson pressure problem expresses all of the extended spatial coupling between nodes during a time step. Since the diagonal dominance is slight for $\Delta t \gg h/c$, this coupling is very strong for large Δt. The efficiency of the TRAC/THERMIT approach results from the fact that this difficult spatial coupling is reduced to a set of relatively few equations of simple form, to which a number of known techniques are applicable[9]; these typically involve inner iterations (for each Newton iteration).

In sum, the technique consists of first reducing from the full set of linearized difference equations to a smaller set of equations for the pressures only; this cell-by-cell reduction accounts for the implicit coupling due to interfacial exchanges. The relatively simple pressure problem which results is then solved applying standard elliptic methods, to account for the extended spatial coupling caused by sonic propagation.

An indication of the effectiveness of this approach is that in THERMIT only one or a very few Newton iterations generally suffice for each time step, whereas (using the line Gauss-Seidel iteration method) 50 or more inner iterations may be required even for a modest sized problem. However, the inner iterations are so rapid that the computing cost of 50 per Newton iteration is barely noticeable.

In contrast to this method, the method of reference 1 essentially performed the Newton and inner iteration simultaneously, so that many costly Newton iterations could be required; and the IMF technique first proposed by Harlow and Amsden[5] actually reversed the order, taking several Newton iterations (cell by cell) for each Gauss-Seidel sweep. This latter method has been found to converge very slowly for some problems such as single-phase liquid flow. We can see that this is to be expected, since Gauss-Seidel iterations are slow to converge when $(h/c\Delta t)^2$ is small, as will be true when c is a liquid sonic velocity. (Cf. reference 10.)

We observe that the strategy of reducing to a Poisson pressure problem with semi-implicit differencing could be extended, following the principles set forth above, to more than two fluids, and should be more efficient than the IMF technique for calculations where $\Delta t > h/c$.

Finally, we would like to make a remark about the reliability of the above solution technique. The inner iterations involve a well-known type of problem. Efficient techniques can be used which converge whenever the problem is diagonally dominant, as can be shown true[3] so long as the individual phase densities and sonic velocities are positive, and $0 \leq \alpha \leq 1$. The Newton iteration technique is also known to converge provided the right hand sides of the difference equations are differentiable in the new time variables, and if the initial guess is close enough to the true solution. In most cases the old time level values provide a good starting guess for Newton iteration. If the iterations should fail to converge, however, the same old time level values provide a better initial guess for solving difference equations with smaller Δt. A built-in automatic time step reduction algorithm can remedy any convergence difficulties which may arise. In practice this is not costly, since time step reduction is usually not necessary; it serves to make the two-fluid field solution technique exceptionally reliable.

HEAT TRANSFER NUMERICAL METHOD

As mentioned above, THERMIT solves the fluid flow equations 1 coupled to fuel rod heat conduction equations via a best estimate heat transfer package. This means constructing a single, continuous boiling curve from recommended correlations[1] to find the heat flux to the coolant in terms of fluid temperatures, wall temperture, and other properties; the fluxes multiplied by surface areas yield the terms Q_{wv} and Q_{ℓ} in equations 1e and 1f. In THERMIT the heat flux to the vapor and to the liquid are given generally as

$$\dot{q}''_{wv} = h_{vc}(T_w - T_v) + \dot{q}''_v, \tag{4a}$$

$$\dot{q}''_{w\ell} = h_{fc}(T_w - T_\ell) + h_{nb}(T_w - T_{sat}) + \dot{q}''_\ell \ . \tag{4b}$$

For $T_w < T_{sat}$ only the liquid forced convection term containing h_{fc} is used, with h_{nb} added for subcooled and nucleate boiling. In the film boiling and single-phase vapor regimes only the h_{vc} term appears. In the transition region (above critical heat flux but below minimum stable film boiling temperature), the recommended correlations do not give heat flux in the usual form of a coefficient times a wall-fluid temperature difference. Therefore THERMIT sets all h's to zero and uses $\dot{q}''_v$ and $\dot{q}''_\ell$ in the transition region.

Since the wall-fluid temperature differences above are often only a few degrees, the heat fluxes are quite sensitive to these temperatures, and their numerical stability is an important consideration. The coefficients h, on the other hand, typically depend less strongly on the correlating variables, and it is usually permissible to calculate the h's for a given time step solely in terms of old time variables without risking instability.

In order to conserve energy, the choice of time levels for the temperatures in equations 4 must be the same in the rod conduction equation as in the fluid dynamics. This means a straightfoward thermal hydraulics solution method would treat either the wall temperature or the fluid temperatures explicitly, as has been done up to now. The numerical stability of this approach depends on whether Δt is less than a characteristic time proportional to a heat capacity divided by the heat transfer coefficient h. With explicit fluid temperature, numerical instability can occur when fluid heat capacity is low (e.g. pure vapor flow); with explicit wall temperature, thin clad walls cause numerical instability. For liquid metal coolant with its strong heat transfer, the problem would be much worse. Of course, stability can always be restored by decreasing Δt. However, since we found typical LWR core problems exhibiting such instability, we have devised a numerical method treating both temperatures implicitly. This means the heat transfer introduces no upper stability limit on Δt, upholding our aim of maximum flexibility in choosing time step size.

Our doubly implicit numerical heat transfer coupling requires more intimate connection between the rod conduction and fluid dynamics stages of the thermal hydraulic calculation. This is mitigated by the fact that equations 4 are already linear in the implicit variables (temperatures). The overall scheme is as follows:

1. At the beginning of each time step, use the old time quantities to determine the heat transfer regime and evaluate appropriate coefficient(s) h.

2. Set up the fuel rod radial conduction problem for each fluid cell; perform the forward elimination of the resulting tridiagonal matrix to obtain T_w^{n+1} as a linear function of the (as yet unknown) new fluid temperatures.

3. Substitute this linear expression for T_w^{n+1} into

$$q_{wv}^{n+\frac{1}{2}} = h_{vc}^n (T_w^{n+1} - T_v^{n+1}) + q_v^{n+\frac{1}{2}}, \tag{5a}$$

$$q_{w\ell}^{n+\frac{1}{2}} = h_{fc}^n (T_w^{n+1} - T_\ell^{n+1}) + h_{nb}^n (T_w^{n+1} - T_{sat}^{n+1}) + q_\ell^{n+\frac{1}{2}} ; \tag{5b}$$

then form Q_{wv} and $Q_{w\ell}$ and solve the fluid dynamics equations.

4. Once new fluid temperatures are known, compute the corresponding new wall temperature, and from that complete the backward substitution of the heat conduction problem to obtain new fuel rod temperatures.

Compared to previous methods, this requires extra effort in two places. The communication between the rod conduction and fluid dynamics steps involves a linear relationship between wall and fluid temperatures, whereas methods explicit in one temperature pass only a fixed temperature. Also, the rod conduction problem must be kept stored in its half-solved state during the fluid dynamics phase. This turns out to require one additional storage word per rod temperature node (per fluid cell).

Since the fluid dynamics method reviewed above already handles Q_{wv} and $Q_{w\ell}$ which are smooth functions of the new fluid temperatures in a given fluid cell, equations 5 pose no special difficulty for the fluid dynamics solution; they are merely more complicated functions of the new time fluid temperatures, expressing the feedback effect of a change in fluid temperature on wall temperature. The only novelty is the construction in step 2 of a linear expression relating T_w and the fluid temperatures.

This turns out to be rather easy. The radial heat conduction equation is discretized to yield a set of finite difference equations with a simple tridiagonal coefficient matrix. Let the first equation be at the rod center node, the Nth at the outer clad surface. This last rod conduction equation looks like

$$c_1 \left(\frac{\rho c_p}{\Delta t}\right) T_N^{n+1} + c_2 (T_N^{n+1} - T_{N-1}^{n+1}) = -q_{wv}^{n+\frac{1}{2}} - q_{w\ell}^{n+\frac{1}{2}} + \ldots$$

where the dots represent terms independent of the fluid temperatures; the difference equations at interior rod nodes are completely independent of fluid temperatures. Therefore, by performing forward elimination of the tridiagonal system, we change the last equation to

$$a\, T_N^{n+1} = h_{fc}^n\, T_\ell^{n+1} + h_{nb}^n\, T_{sat}^{n+1} + h_{vc}^n\, T_v^{n+1} + \ldots .$$

Since $T_N^{n+1} = T_w^{n+1}$, this is precisely the linear relationship needed for step 3.

We have so far concentrated on the heat flux terms involving h_{vc}, h_{fc}, and h_{nb}, glossing over the transition regime heat flux terms in equations 5. Our new numerical technique also permits an improved representation of these terms. When the transition regime is reached, heat flux becomes relatively insensitive to the fluid temperatures; however, it now decreases strongly with increasing wall temperature. Thus the boiling curve (heat flux vs. temperature difference) has negative slope in transition boiling, contrary to other regimes. Previous heat transfer methods which treated wall temperature explicitly (e.g. reference 2) were unable to represent this negative slope during a given time step. Our method now permits us to approximate the transition region heat flux correlations by straight lines having the correct negative slope during each time step. The formulas given above are therefore slightly more complicated; for further details see reference 3. In examples below, we shall demonstrate how this negative slope treatment can significantly improve numerical accuracy in the transition boiling regime.

APPLICATIONS

The remainder of this paper presents representative applications of the THERMIT code to LWR core thermal hydraulics problems. The problems are of less than realistic complexity; their purpose is to demonstrate selected aspects of THERMIT's capabilities. The first two also serve as benchmarks.

CROSSFLOW EXPERIMENT INTERPRETATION

One of the most important features of the THERMIT code is the three-dimensional flow modelling, which was developed specifically for application to interbundle crossflow. To test the validity of the THERMIT approach, we have compared calculations against proprietary data obtained at Babcock and Wilcox[1,2] in isothermal two-bundle tests. The experimental apparatus consisted of two bundles of simulated fuel pins; the bundles were separated above and below a common mixing length by divider plates. Each bundle inlet flow rate could be adjusted separately. If we define the inlet flow rate upset to be the difference of the two inlet flow rates divided by the larger one, the data analyzed correspond to inlet flow upsets of 0.05, 0.25, and 1.

Measurements were made of the flow velocities upstream and downstream of the test section, and of local pressures at various axial levels and transverse positions in the test section. Each of the two bundles was an 8x15 rod array; together as an 8x30 array they simulated the full width and about half the thickness of two side-by-side bundles. Axially the test section contained three spacer girds, and pressure taps (inside the various rods) at nine levels. Each bundle had a complete set of pressure taps in each of three 8x5 rod subregions. At each axial level pressures were measured from two rods in each of the six transverse subregions. There may be some uncertainty due to the fact that within a given subregion, taps were placed in different rods (and hence slightly different transverse locations) for different axial levels.

Although the eventual figure of merit in LWR interbundle crossflow analysis would probably be crossflow velocity, for analysis of these experiments we shall place greater emphasis on transverse pressure profiles. We do this for two reasons. First, in a real LWR, crossflow tends to follow in a complex inter-

relationship with driving pressure forces. But in this experiment the inlet velocities are imposed, so here it is more a case of pressures determined by velocities. Second, the data actually obtained in the experiments were the pressures; B&W also supplied crossflow velocity data, but these were inferred from the pressures under certain analytical assumptions. We therefore chose pressure data as the most meaningful yardstick for these comparisons.

Most calculations reported here were carried out on a space mesh six intervals across (one per subregion) and twenty intervals in the axial direction. We ran calculations with THERMIT, and also with the codes COBRA IIIC/MIT[13] and COBRA IV-I[14], both of which use an identical crossflow model different from the one in THERMIT. Recall that THERMIT uses momentum equations containing all transverse momentum convection terms, and an empirical correlation for pressure drop in transverse flow across tube banks; we chose a standard off-the-shelf correlation due to Gunter and Shaw[15] which was incorporated in THERMIT without modification. Both COBRA codes neglect certain convection terms in the momentum equation, and use a special pressure drop term developed specifically for this application; they also include turbulent momentum mixing terms not in THERMIT. For the COBRA crossflow model, empirical constants K_{ij} and s/l need to be supplied; we chose the recommended default value of 0.5 for both. The numerical techniques in the COBRA codes are somewhat different, but each uses a steady-state marching method requiring positive axial flows which are assumed to be large compared to the crossflows. THERMIT transient calculations were performed using the maximum (convective limit) time step size repeatedly until a steady flow was attained.

The first two figures pertain to the mildest case of 0.05 inlet flow upset. Figure 1 shows the ratio of axial velocity in the low flow to the high flow bundle, as a function of axial position; recall that the solid line is an indirect inference from the data. Agreement of all three codes with inferred data is good, the largest deviation being 2%. THERMIT predictions are closer than COBRA predictions in the first half length, less close in the second. Figure 2 shows transverse pressure differences versus axial position for the same case. The ordinate is found by subtracting the average pressure in the three low flow subregions from the average pressure in the three high flow subregions, then normalizing by a reference pressure. The continuous curve representing experimental data is based on a spline interpolation done by B&W. COBRA IIIC/MIT gives quite good predictions of the transverse pressure difference; THERMIT is reasonably good, except behind the second grid. The COBRA IV-I predictions show the largest deviations from the data, even though COBRA IV-I uses the same physical model as COBRA IIIC/MIT.

The next figure illustrates results for the intermediate case of 0.25 inlet flow upset. Figure 3 shows the axial velocity ratios, with all codes agreeing closely with the data. THERMIT does not overpredict this ratio in the second half length for this case. Fugure 4 shows the pressure difference predictions. This time COBRA IV-I is better than COBRA IIIC/MIT; THERMIT is as good as COBRA IV-I except behind the second grid.

The two cases exhibit an inconsistency of results with the COBRA codes. Even though both codes purport to use the same physical model for crossflow, they give quite different results, and either code may be poorer than the other. A more startling inconsistecy involves axial mesh size: when the axial mesh was refined to 36 intervals, both COBRA IIIC/MIT and COBRA IV-I gave results very different from the predictions with 20 axial intervals. The differences are most strikingly

apparent in the crossflows; Figure 5 shows crossflow vs. axial position for 6x20 and 6x36 interval meshes using COBRA IV-I. Similar though less extreme behavior was observed with COBRA IIIC/MIT. Furthermore, when the axial mesh was further refined to 72 intervals, both codes failed to converge.

In contrast to this highly disturbing behavior of both COBRA codes, THERMIT calculated consistent and converging crossflows for 20, 36, and 72 axial intervals, as shown in Figure 6.

Returing to the 6x20 mesh results, we see in Figures 7 and 8 a more detailed view of pressures for the 0.25 inlet flow upset case. Transverse pressure profiles (in the six subregions) are given for two axial levels, with each curve normalized to have the same average pressure. Figure 7 corresponds to relative axial position 0.25 just upstream of the first grid, where the trends are well matched by all three codes. Figure 8 shows a more confused picture at relative axial position 0.33 just past the first grid; the central depression in the data curve seems to be due to some factor not accounted for by any of the calculations. Nevertheless, THERMIT predicts the overall trend reasonably well, as does COBRA IV-I, while COBRA IIIC/MIT misses the trend.

So far we have not mentioned a special feature of THERMIT crossflow modelling near spacer grids. Physically we might expect a spacer grid would tend to funnel slanted fluid velocities into more purely axial velocity as fluid passes through a grid. Because THERMIT includes all multidimensional convection terms in the mementum equations, it is possible to model this funnel effect of the grid by reducing the term representing axial convection of transverse momentum downstream of the grid. THERMIT presently contains an all-or-nothing funnel effect option which allows the user to specify whether this term is kept intact or dropped entirely at the node downstream of any spacer grid. THERMIT calculations above were carried out with the funnel effect at all grids. Figure 9 shows the same pressure data as Figure 4 for THERMIT with the funnel effect, compared to a THERMIT calculation without the funnel effect. The funnel effect impoves predictions in this case at the first grid, but is less good for the second and third grids. A better funnel effect model might therefore allow for partial transverse momentum loss at a grid, with proportionately more loss where crossflow is stronger. Figure 10 shows the influence of funnel effect on calculated crossflow. (We remind the reader that the data curve in Figure 10 is inferred indirectly and may not be valid for judging which prediction is better.)

The third experimental case considered had an inlet flow upset of 1; this means there is no flow entering one of the bundles. This exceeds the range of validity of both COBRA codes: not only is crossflow here of the same magnitude as axial flow, but due to a recirculating flow pattern near the inlet there are negative axial flows at some points. Both COBRA codes failed to converge for this problem.

THERMIT can model this case; calculations were performed which showed a recirculating flow pattern at the inlet of the zero inlet flow bundle. Figure 11 shows the resulting THERMIT axial velocity ratio predictions; agreement is good in the first half length, with a maximum 8% deviation in the second half length. The pressure difference is shown in Figure 12. THERMIT overpredicts the pressure difference near the inlet; this might be reduced somewhat if a finer transverse mesh were used.

These experimental analyses show that at least for the 6x20 mesh all three codes - COBRA IIIC/MIT, COBRA IV-I, and THERMIT - are in close agreement with each other and in fairly good agreement with experimental data. This is perhaps surprising, and certainly encouraging, since the empirical crossflow model in the COBRA codes has benefitted from extensive efforts of adjustment for a highly specific application, whereas THERMIT used a general, off-the-shelf correlation without any modification. The predictions of COBRA IIIC/MIT and COBRA IV-I differ more than one might expect given that they use the same physical model. The sensitivity of both codes to axial noding is disturbing, since there are no rules for choosing a proper axial mesh.

Comparing THERMIT with the COBRA codes also reveals that turbulent mixing effects appear much less important for subregion analysis than would be true for subchannel analysis. The results indicate that momentum flux modelling based on pressure differences is of primary importance when using transverse nodes larger than subchannel size.

TWO-PHASE FLOW DECAY TRANSIENT

Our next example is a flow decay transient with boiling; under certain simplifying assumptions Gonzalez-Santalo and Lahey [16] obtained an exact solution in one space dimension for such a transient. The simplifying assumptions were basically that the heat flux is constant in both space and time, that the homogeneous equilibrium model for two-phase flow is used, and that the phase densities be constant. The analytic solution was obtained for the case that the inlet flow rate is a given exponentially decaying function of time.

Our calculation of this example serves two important purposes. One is to verify the correct and accurate treatment of continuity and energy balance as programmed in THERMIT. (The momentum equations are not so tested, because the analytic soltuion is independent of the pressure drop.) The second is to demonstrate the ability of the THERMIT numerical method to simulate the homogeneous equilibrium model of two-phase flow via the two-fluid model. This was accomplished by furnishing very large values for coefficients in the interfacial momentum, energy, and mass transfer terms. Only a numerical method which treats interfacial exchanges implictly could handle arbitrarily large exchange coefficients without reducing time step size. In other words, the THERMIT two-fluid model can be reduced to the homogeneous equilibrium model without additional penalty if so desired.

The problem calculated[16] involved flow in a heated pipe with inlet flow decaying on a 3-second period. Flow was saturated at the inlet at all times, and a constant system pressure of 1000 psia was assumed. The THERMIT calculation was not a precise simulation of the problem of Gonzalez and Lahey, since THERMIT treats both phases as compressible; however these differences should be slight.

Figures 13 and 14 compared quality and mass flow rate points calculated by THERMIT with the analytic solution curves published in reference 16. The same problem was also calculated by COBRA IV-I; those results were publiched in reference 14. The THERMIT results agree even more closely with the analytic solution than did COBRA's which were already excellent.

BWR ROD DROP ACCIDENT

This example is a simple one-dimensional model of the thermal hydraulic behavior in a hot channel during a rod drop accident at hot standby conditions. The power burst which drives this transient was taken from a three-dimensional coupled kinetics and thermal hydraulics calculation [7] and supplied to THERMIT as input. Initially the coolant is at rest at a temperature a few degrees below saturation. When the power burst begins to transfer heat to the coolant, subcooled void forms and builds up pressure in the channel. Since the channel is open at both ends, fluid would probably be expelled out the top and out the bottom as vapor continues to form inside.

Previous core thermal hydraulics codes such as COBRA IIIC have been limited in modelling such a transient by numerical solution methods which do not permit negative axial flow. Thus the best one could do for this transient was to specify a very small positive inlet flow throughout the transient. THERMIT, on the other hand, uses a numerical method which can treat reversed flow. THERMIT also can accept more general types of boundary conditions; given velocities or given pressure histories can be set at the inlet or the outlet. (A more general relationship coupling flow rates and pressure drops could also be handled by the numerical methods.) We calculated our BWR rod drop accident model[2] with THERMIT using two different types of boundary conditions to check their influence. One was fixed zero inlet flow, as would have to be used with COBRA IIIC; the second was a constant pressure drop across the channel, resulting in a nearly symmetric expulsion out both ends.

The different boundary conditions gave significantly different results in important calculated quantities. The zero inlet flow calculation showed fluid being expelled from the outlet, with velocities at any given time increasing from zero at the inlet to large velocities at the outlet. Consequently, the peak heat flux at the core midplane was deposited into a rapid fluid flow. On the other hand, with the pressure drop boundary condition, fluid was expelled nearly symmetrically, so it was nearly stagnant in the middle of the channel where heat flux was highest. As a result, transient CHF was predicted much earlier for the second case. This is reflected in the peak wall temperature histories of Figure 15.

The most realistic boundary condition for this problem would probably be something between the two extremes considered here, since the inlet flow orifice would somewhat restrict expulsion from the inlet. The purpose of this example was to demonstrate that core flow boundary conditions can have a material influence on calculated thermal hydraulic behavior. Many other types of transients may be sensitive to such boundary conditions; a careful study of sensitivity and investigation of physically correct boundary conditions appears warranted. A major advantage of the THERMIT numerical method is that it can handle very general boundary conditions to carry out a sensitivity study, and to implement whatever form of boundary condition is ultimately required.

PWR MULTICHANNEL STEADY STATE

In calculating some typical PWR core thermal hydraulic problems, we discovered that at nominal conditions an explicit treatment of wall temperatures in the heat flux from fuel rod to coolant led to serious numerical stability problems. This example is a cluster of nine PWR channels in a symmetric 3×3 array, with relative assembly powers of 1.6 in the central channel, 1.3 in the four side channels, and 1 in the four corner channels. Once a thermal hydraulic steady state had been established

it was found that, using explicit wall temperatures in equations 4, in order for successive time steps to maintain a stable steady state Δt had to be less than 10 msec. This was very restrictive, since the convective limit value was about 70 msec; time steps of the latter size resulted in the oscillating wall temperature instability shown in Figure 16. When the new doubly implicit heat transfer method was implemented, wall temperatures remained stable when Δt was chosen at the convective limit.

POST-CHF HEAT FLUX

This example illustrates the gain in numerical accuracy due to the negative slope heat flux method in the transition boiling regime which was made possible by the doubly implicit heat transfer coupling. The example itself is a typical BWR nominal flow subjected to a transient increase in power sufficient to attain critical heat flux.

Figure 17 shows the heat flux in the cell which first reaches CHF. Two different calculation methods have been used. One is the negative slope method associated with our new numerical heat transfer technique; this method approximates the boiling curve during each time step by a straight line having the correct negative slope in the transition region. The other is a positive slope method used originally in the TRAC[2] code, for example; this method approximates the boiling curve in all regimes by a straight line having positive slope, even though it is incorrect in the transition region. Two curves in Figure 17 show the heat flux calculated by each method with time steps determined by the fluid convection limit. A third curve was calculated with the negative slope method and time steps four times smaller; for purposes of numerical comparison this can be considered nearly exact. The negative slope method with larger time steps falls much closer to this curve than the positive slope method. Note that over the first time step after CHF, heat flux with the positive slope method actually continues to increase. The results confirm our expectation that the negative slope method is numerically more accurate. Figure 18 shows the influence of this difference on wall temperature predictions.

Further comparisons against experimental data are planned to study the effect of the negative slope method on physical predictions.

CONCLUSIONS

The THERMIT code was written to provide improved simulation of three-dimensional thermal hydraulic transients in LWR cores. The code uses a two-fluid model for two-phase flow permitting more physically correct transient modelling which takes on increased importance when reactor kinetics feedback is considered. The numerical fluid dynamics method, adapted from TRAC, has been put on a firm mathematical basis and offers exceptional reliability. It also permits more general three-dimensional flow capability so that reversed flow, flow blockages, and general boundary conditions can be treated. A new numerical heat transfer technique provides desirable additional numerical stability, and permits more consistent and accurate treatment of post-CHF heat flux. Studies performed so far indicate the following:

1. Interbundle crossflow can be predicted well with the multi-dimensional flow model in THERMIT; agreement with experimental data using an off-the-shelf transverse pressure drop correlation in THERMIT compares favorably with results obtained from the carefully adjusted special model in the COBRA codes.

2. Turbulent mixing effects are less significant with assembly-size control volumes than in subchannel analysis.

3. The numerical consistency of THERMIT contrasts with the observed sensitivity of COBRA crossflow results to axial node size.

4. The THERMIT approach handles cases like inlet flow blockage and phenomena such as the funnel effect of spacer grids which the COBRA codes cannot.

5. The choice of core flow boundary condition possible with THERMIT can significantly influence predicted transient thermal hydraulic behavior; the question of physically correct boundary conditions deserves further attention.

6. Some current methods of calculating post-CHF heat flux may introduce errors due to their numerical representation of the heat flux in the transition region.

Future development efforts are planned to include more testing of THERMIT against a range of experimental data, adjustment of models as needed, and hopefully feedback coupling with a multidimensional reactor kinetics code. This should lead to improved simulation of a broader range of core thermal hydraulic transients.

ACKNOWLEDGEMENTS

The authors thank J. Loomis, who calculated the crossflow experiments, and A. Schor, who ran the flow decay problem. We are grateful to Babcock and Wilcox for permission to use their experimental data.

REFERENCES

1. D. R. Liles and Wm. H. Reed, "A Semi-Implicit Method for Two-Phase Fluid Dynamics," J. Comp. Physics 26 (1978), 390.

2. TRAC-P1: An Advanced Best Estimate Computer Program for PWR LOCA Analysis, Los Alamos Scientific Laboratory LA-7279-MS, Vol. I, June 1978.

3. Wm. H. Reed and H. B. Stewart, THERMIT: A Computer Program for Three-Dimensional Thermal-Hydraulic Analysis of Light Water Cores, Electric Power Research Institute report, in press.

4. J. R. Travis, F. H. Harlow, and A. A. Amsden, "Numerical Calculation of Two-Phase Flows," Nucl. Sci. Eng. 61 (1976), 1.

5. F. H. Harlow and A. A. Amsden, "Numerical Calculation of Multiphase Fluid Flow," J. Comp. Physics 17 (1975), 19.

6. M. Ishii, Thermo-Fluid Dynamic Theory of Two-Phase Flow. Eyrolles, Paris, 1975.

7. D. S. Rowe, COBRA IIIC: A Digital Computer Program for the Steady-State and Transient Analysis of Rod Bundle Nuclear Fuel Elements, Batelle Pacific Northwest Laboratories BNWL - 1962, March 1976.

[8] D. R. Liles, these Proceedings.

[9] R. S. Varga, Matrix Iterative Analysis. Prentice-Hall, Englewood Cliffs, NJ, 1962.

[10] H. B. Stewart, "Calculation of Transient Boiling Flow in Channels," J. Comp. Physics, in press.

[11] T. A. Bjornard, Blowdown Heat Transfer in a Pressurized Water Reactor, Ph.D. Thesis, Department of Nuclear Engineering, Massachusetts Institute of Technology, August 1977.

[12] J. R. Gloudemans, Private Communication dated January 24, 1977.

[13] R. W. Bowring and P. Moreno, COBRA IIIC/MIT Computer Code Manual, Department of Nuclear Engineering, Massachusetts Institute of Technology, March 1976.

[14] C. W. Stewart, C. L. Wheeler, et al., COBRA IV: The Model and the Method, Batelle Pacific Northwest Laboratories BNWL - 2214, July 1977.

[15] A. Y. Gunter and W. A. Shaw, "A General Correlation of Friction Factors for Various Types of Surfaces in Crossflow," ASME Transactions 67 (1945), 643.

[16] J. M. Gonzales-Santalo and R. T. Lahey, Jr., "An Exact Solution for Flow Transients in Two-Phase Systems by the Method of Characteristics," ASME Transactions Journal of Heat Transfer (1973), 470.

[17] J. U. G. Valente, Multidimensional Modeling of the Rod Drop Accident, M.S. Thesis, Department of Nuclear Engineering, Massachusetts Institute of Technology, April 1976.

Figure 1. Comparison of Bundle Axial Velocity Ratios for 0.05 Upset Case

Figure 2. Comparison of Normalized Pressure Differences for 0.05 Upset Case

Figure 3. Comparison of Bundle Axial Velocity Ratios for 0.25 Upset Case

Figure 4. Comparison of Normalized Pressure Differences for 0.25 Upset Case

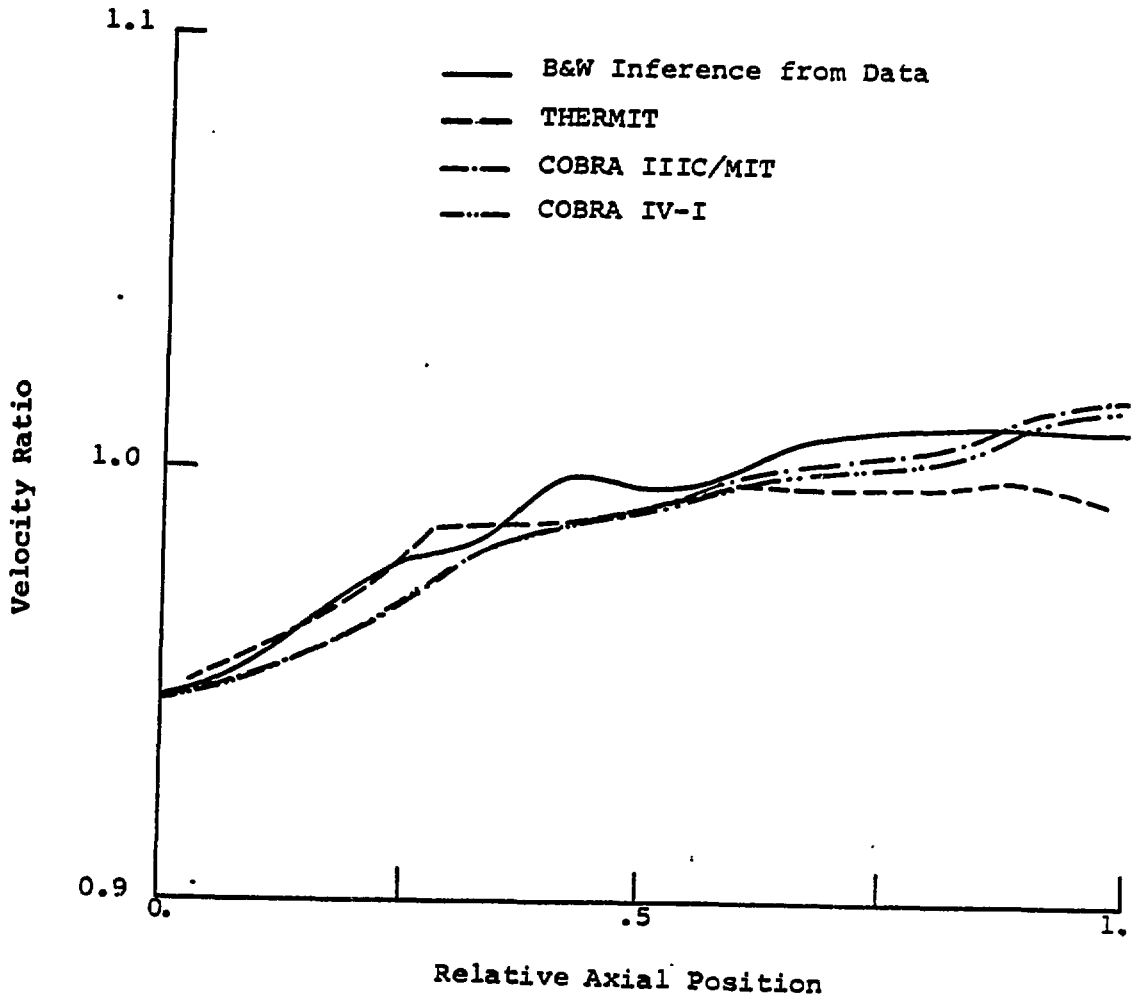
1.1
1.0
0.9
Velocity Ratio
B&W Inference from Data
THERMIT
COBRA IIIC/MIT
COBRA IV-I
0.
.5
1.
Relative Axial Position

Sheet W-14

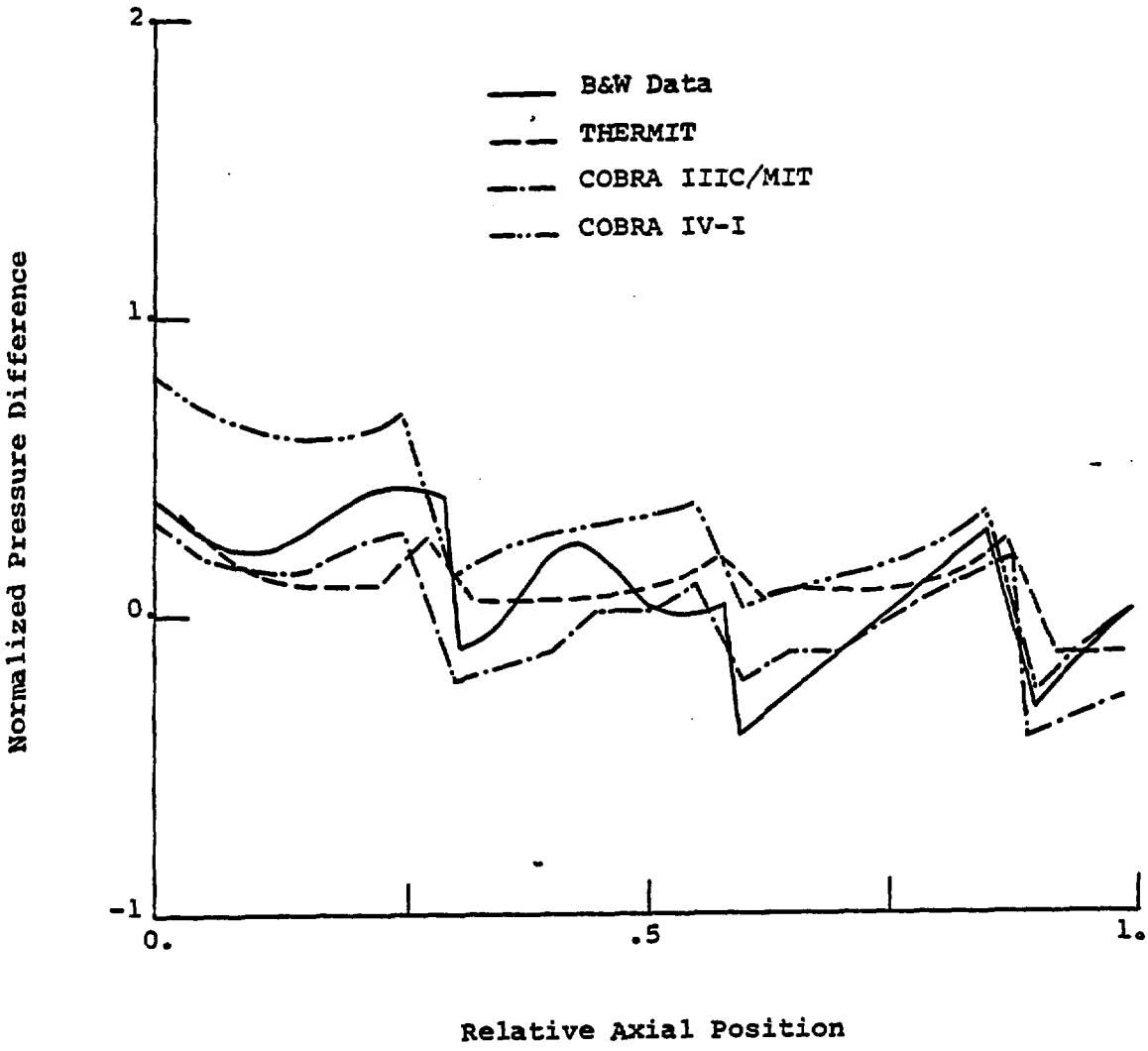
B&W Data
THERMIT
COBRA IIIC/MIT
COBRA IV-I
Normalized Pressure Difference
2
1
0
-1
0.
.5
1.
Relative Axial Position

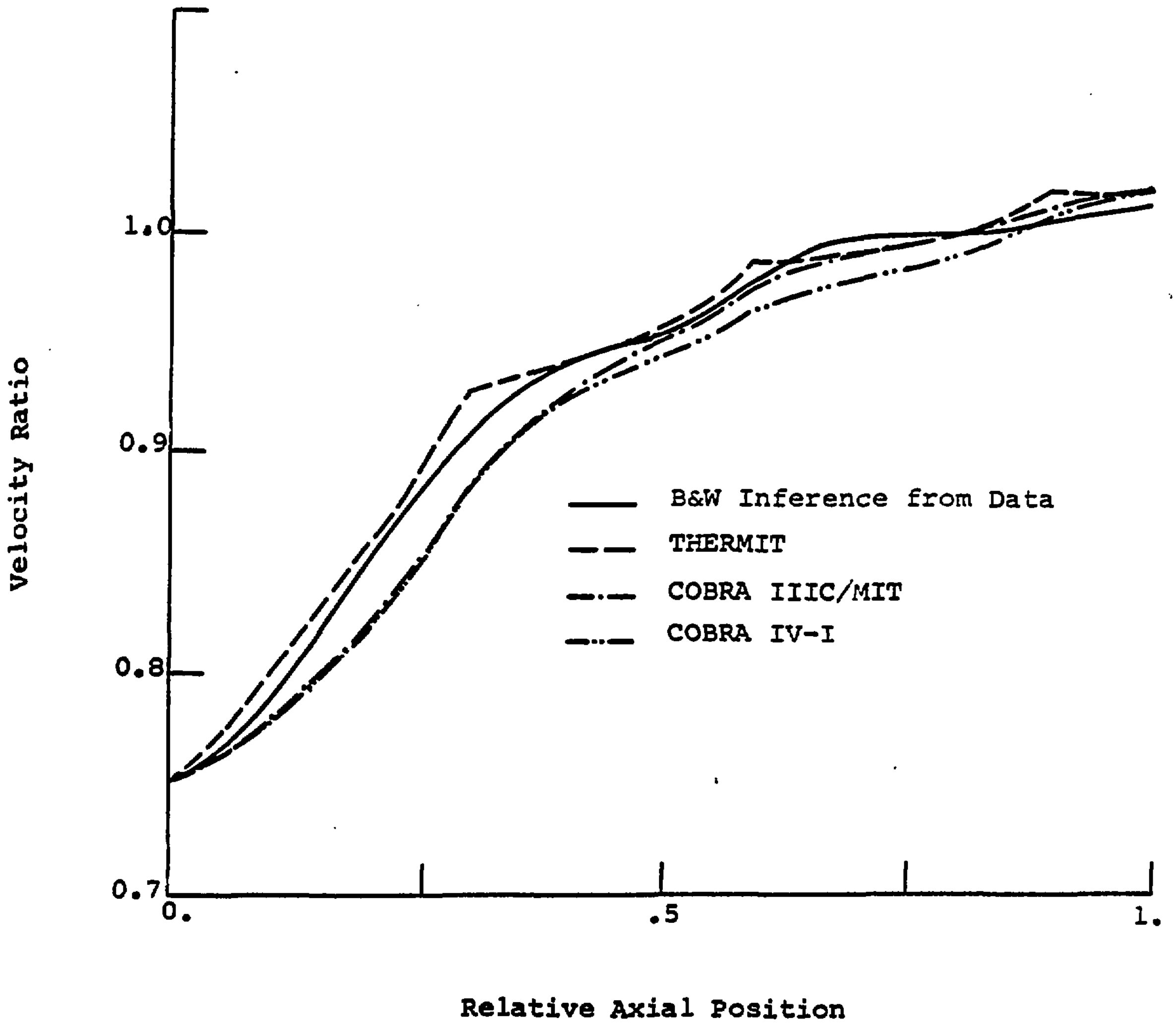

Reed, Stewart, Wolf

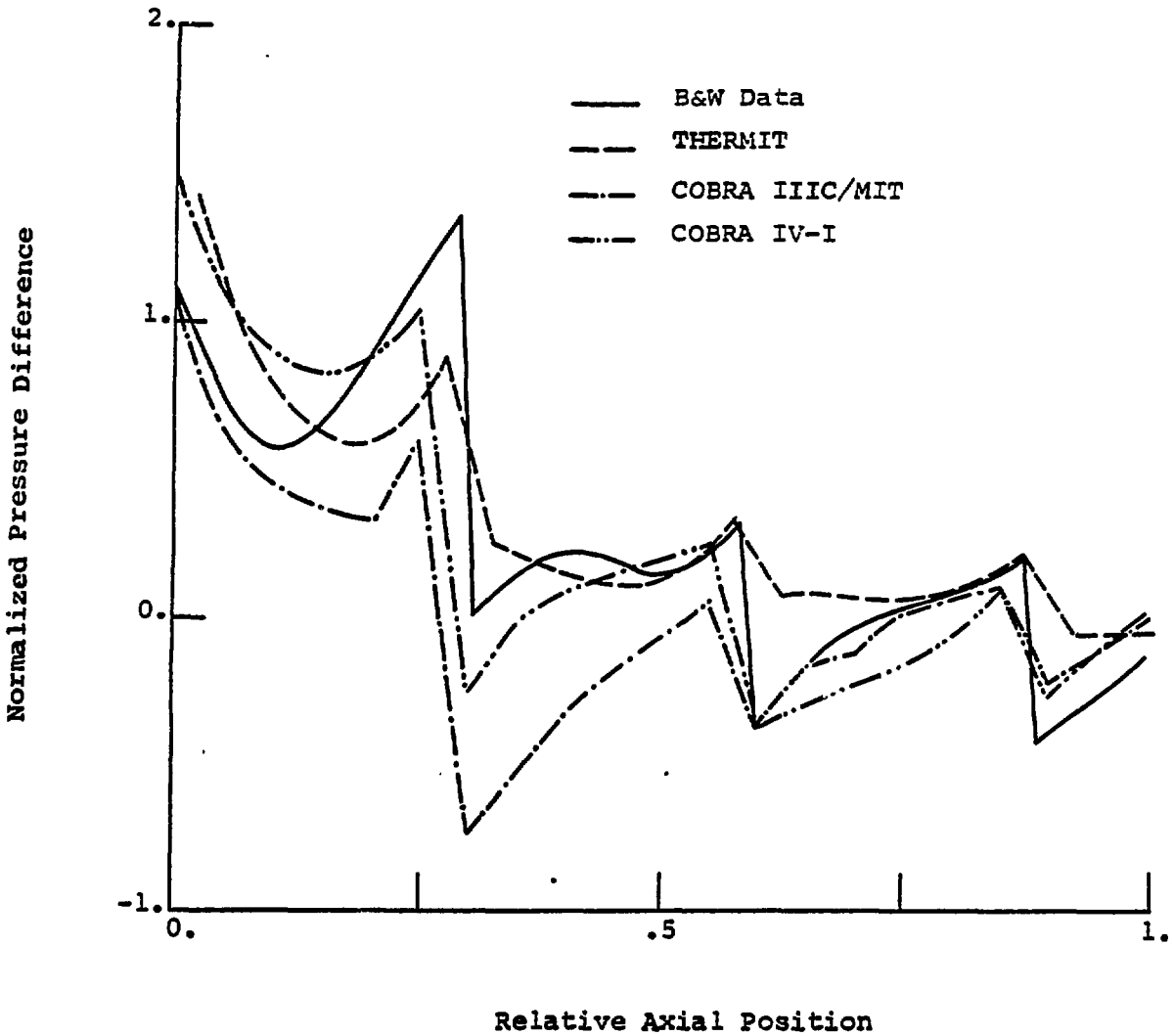

Lead, Stewart Wall

Figure 5. Normalized Crossflow Calculated by COBRA IV-I with Different Axial Noding

Figure 6. Normalized Crossflow Calculated by THERMIT with Different Axial Noding

Figure 7. Transverse Profile of Relative Pressure Before First Grid for 0.25 Upset Case

Figure 8. Transverse Profile of Relative Pressure After First Grid for 0.25 Upset Case

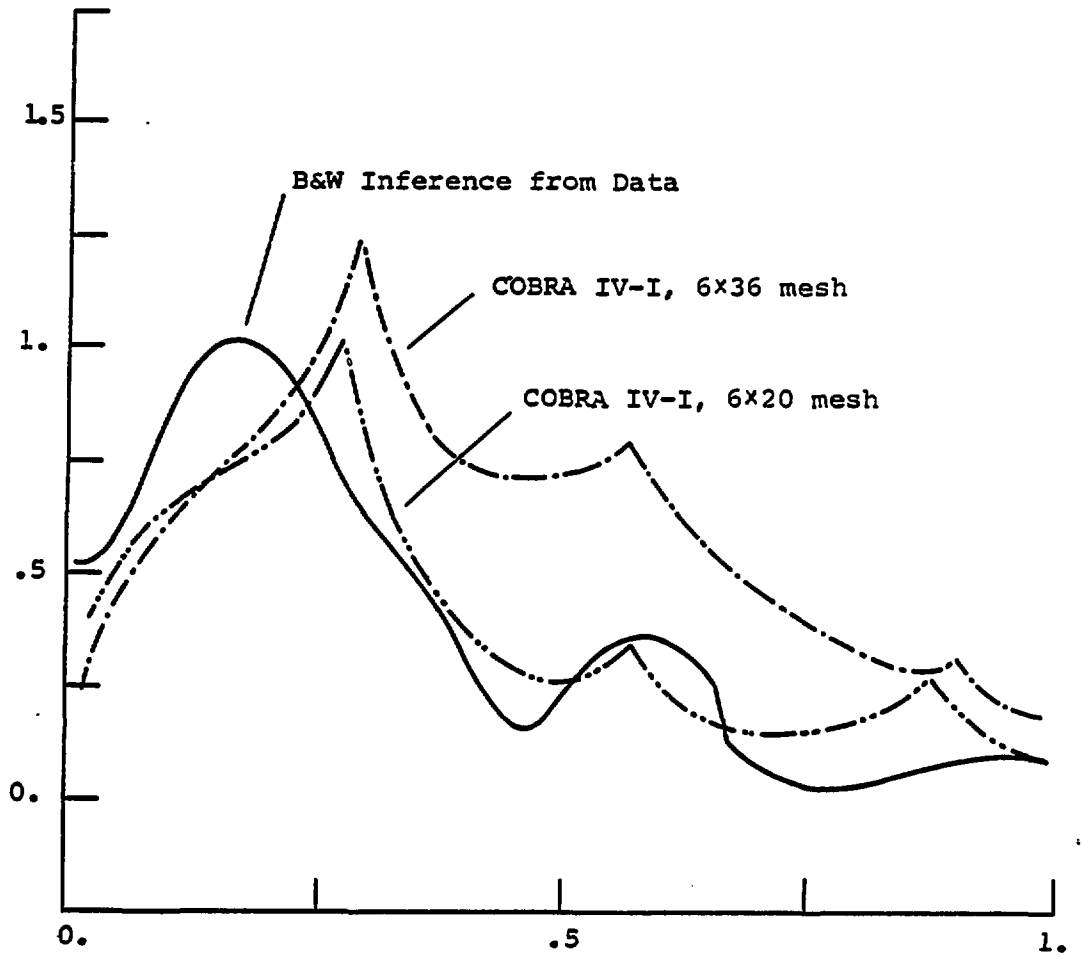

Reed, Stewart, Wolf

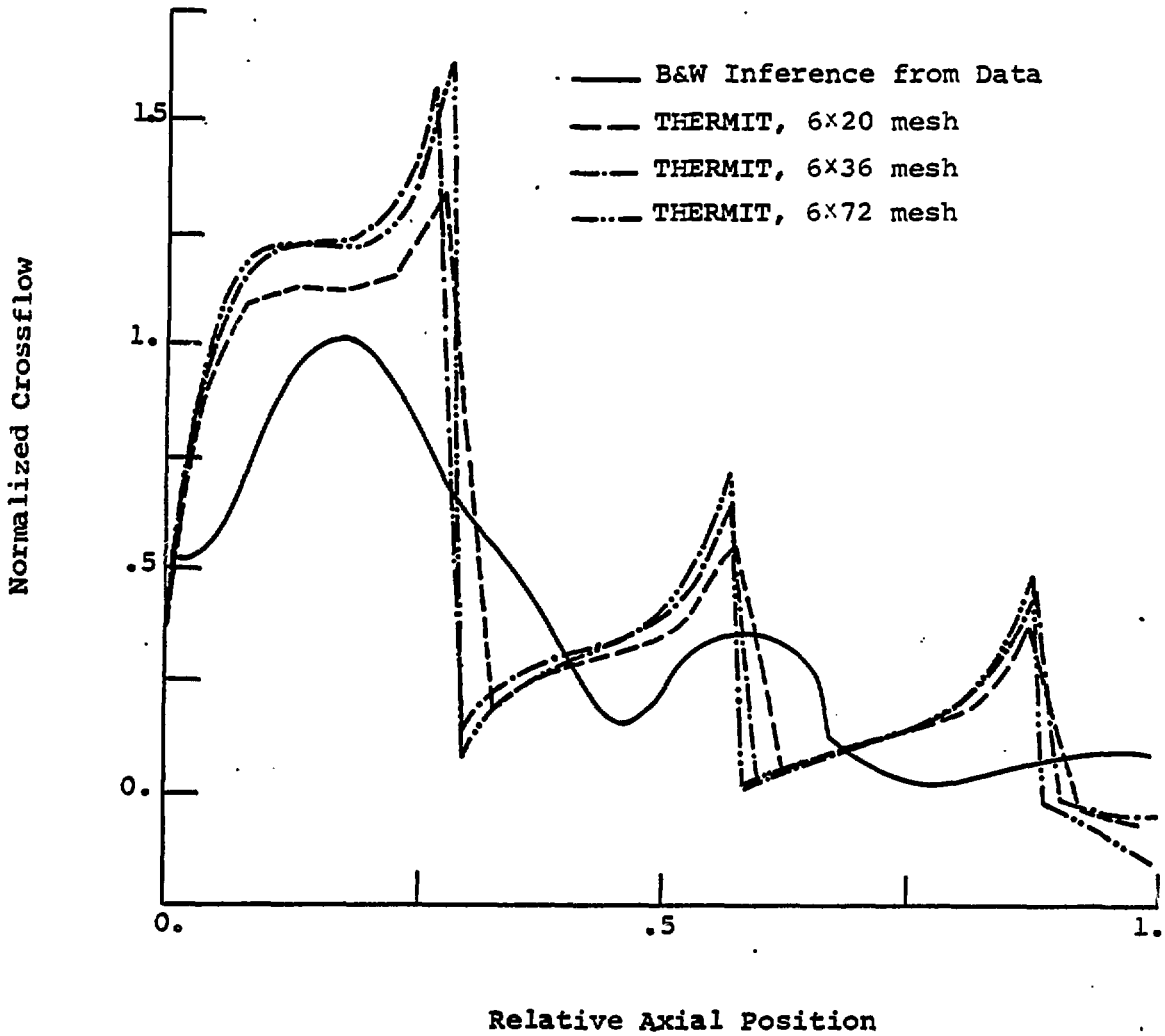

Reed, Stewart, W.I.E

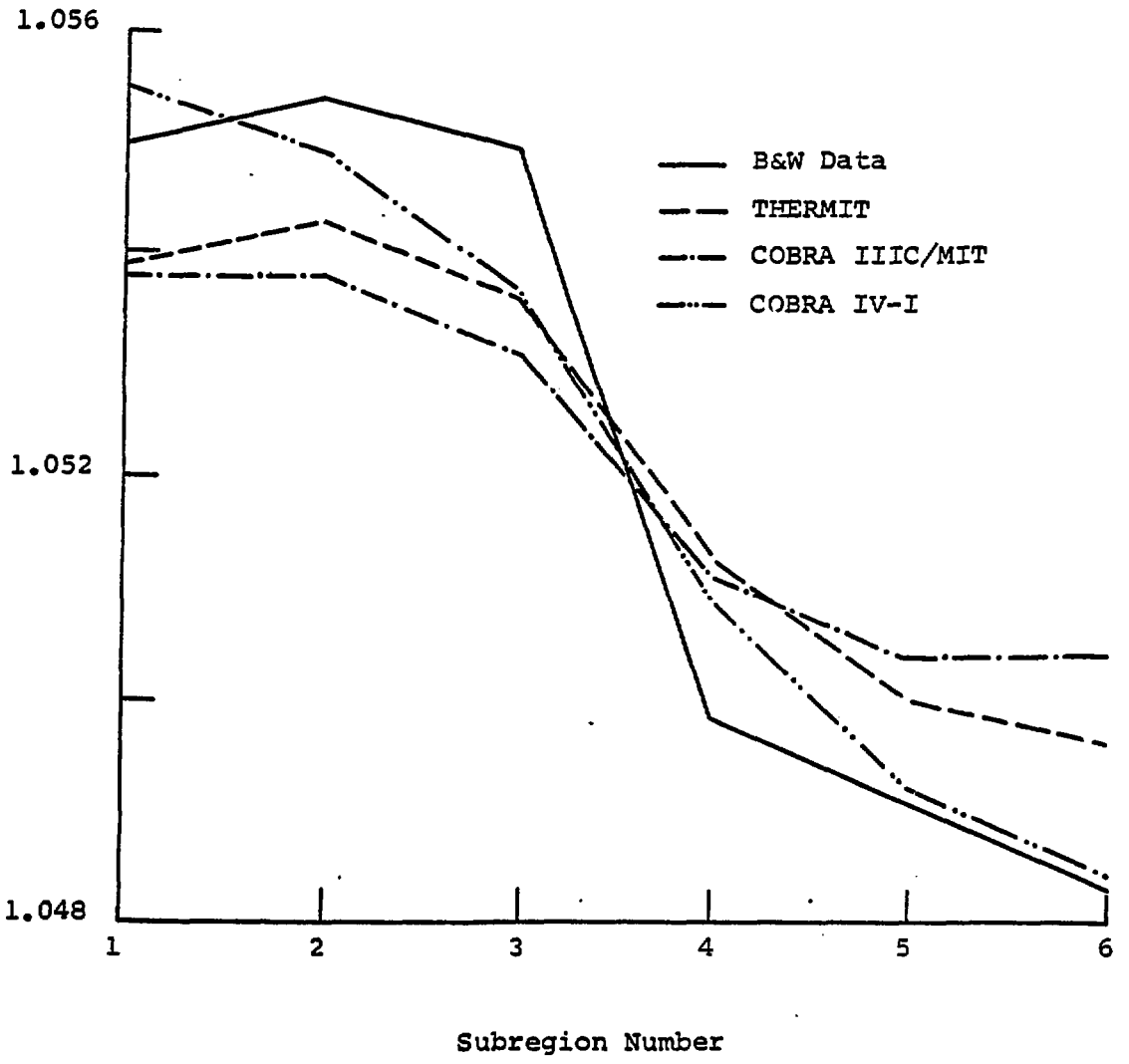

Reed, Stewart, Wolf

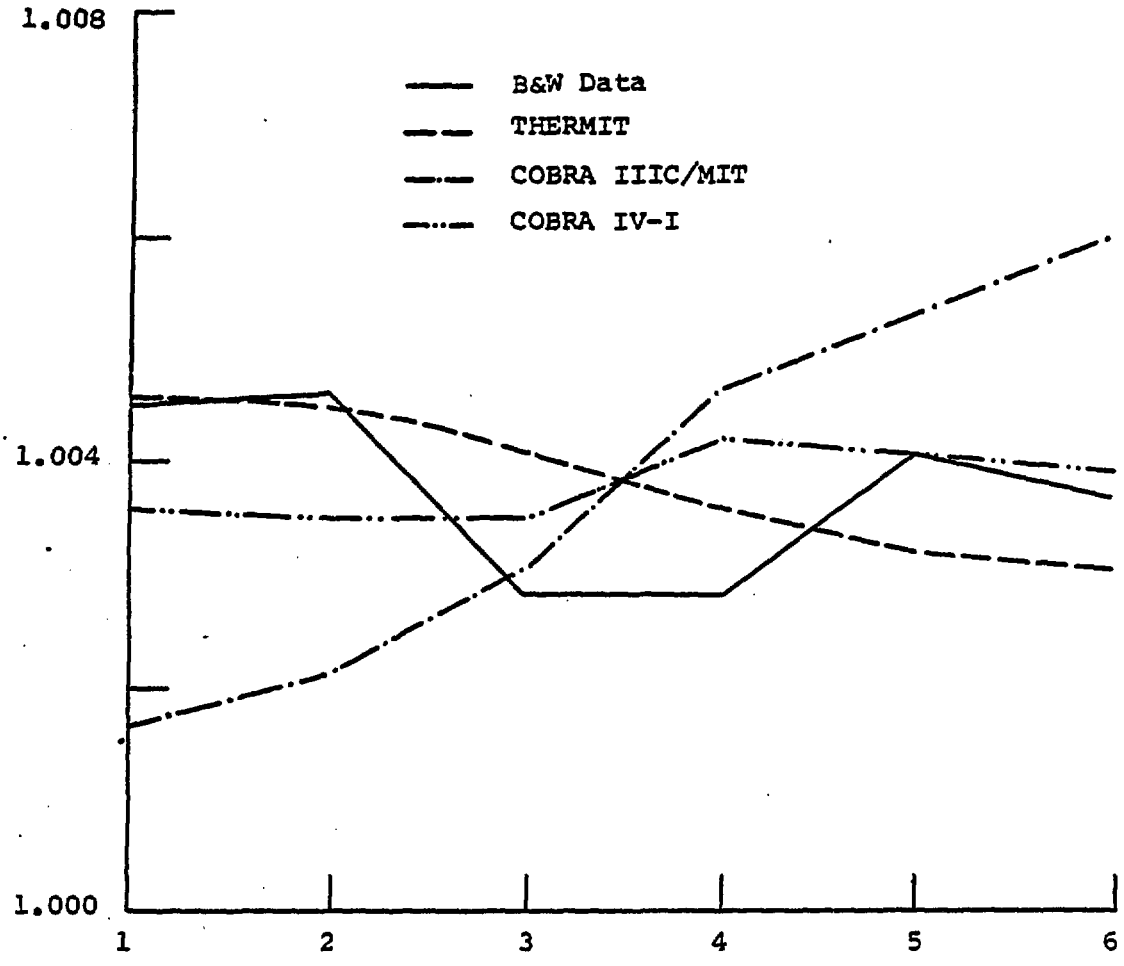

Reed. Stewart, Wolf

Figure 9. Influence of Funnel Effect on Crossflow Predicted for 0.25 Upset Case

Figure 10. Influence of Funnel Effect on Pressure Difference Predicted for 0.25 Upset Case

Figure 11. Comparison of Bundle Axial Velocity Ratios for 1.0 Upset Case

Figure 12. Comparison of Normalized Pressure Differences for 1.0 Upset Case

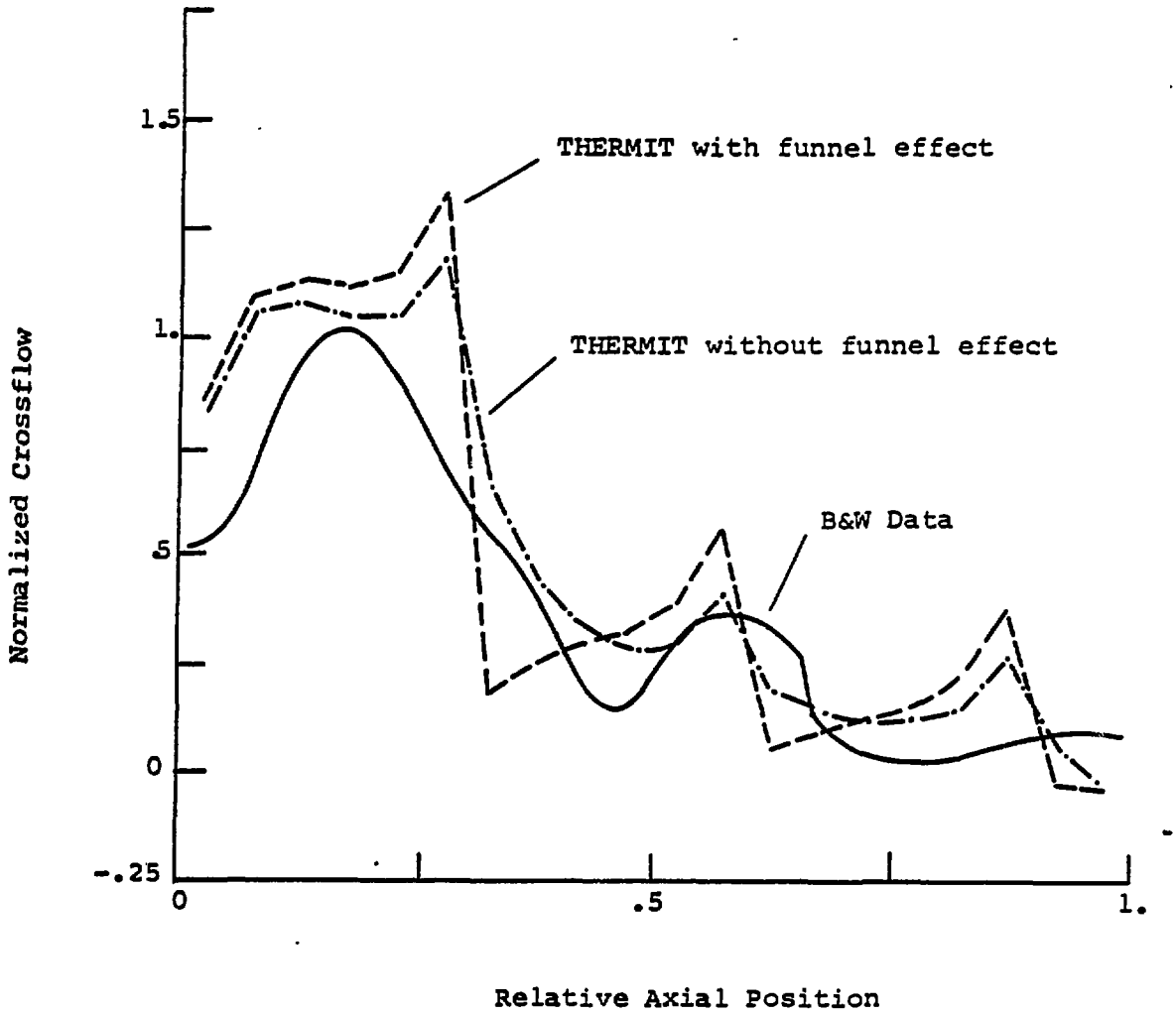

Rec'd Stewart, Wolf

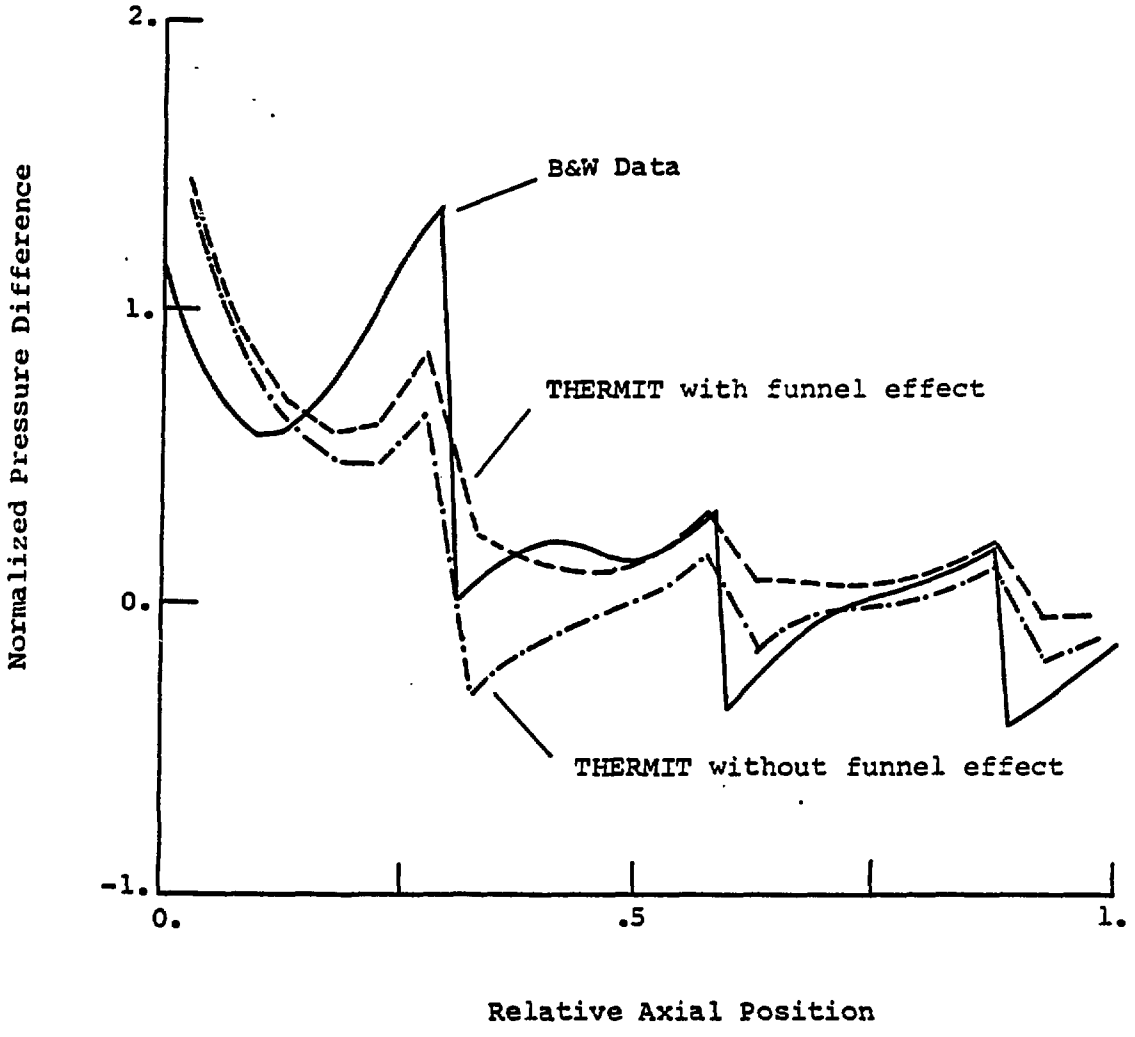

Reed, Stewart, Wolf

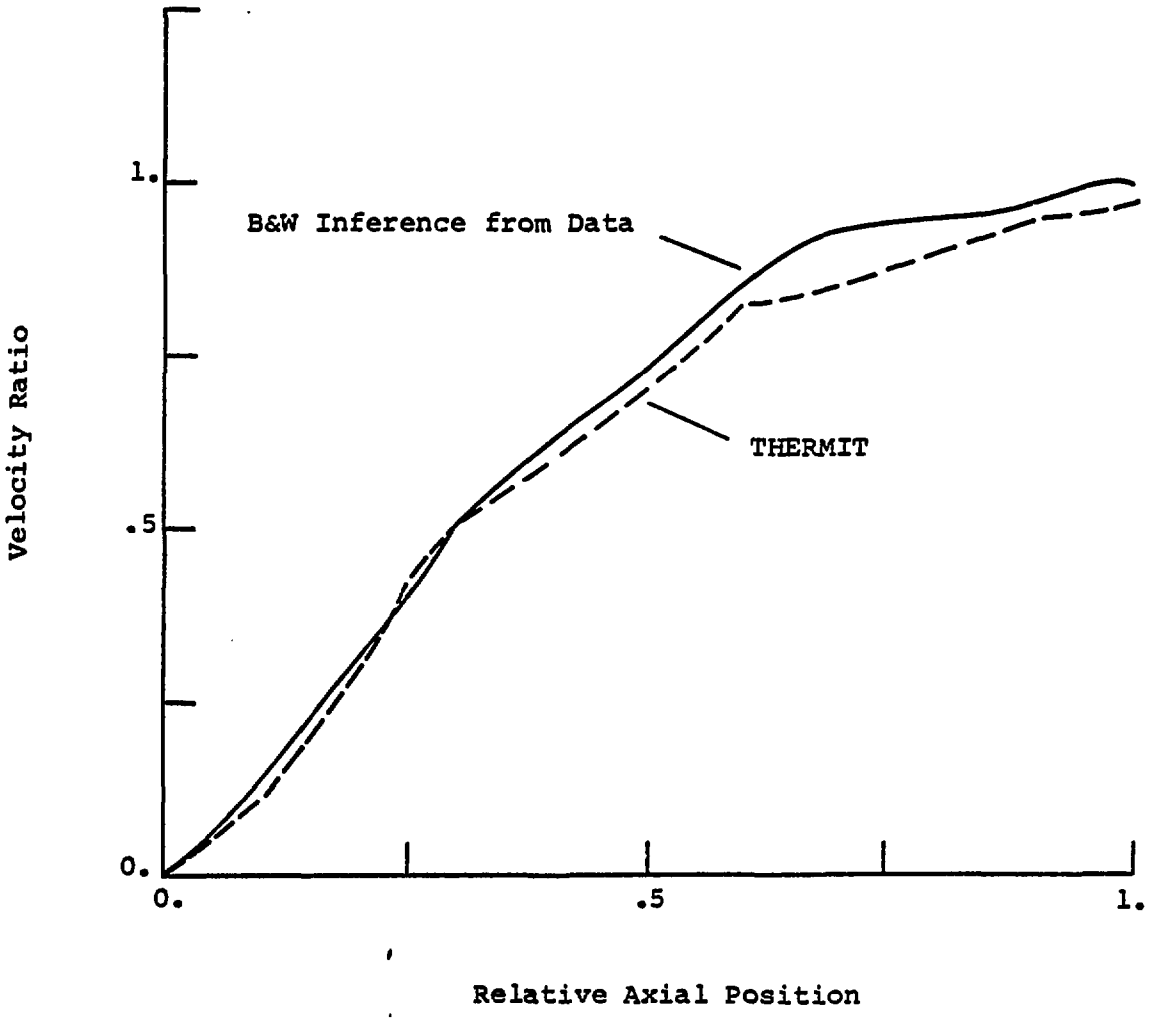

Reed, Stewart, Wolf

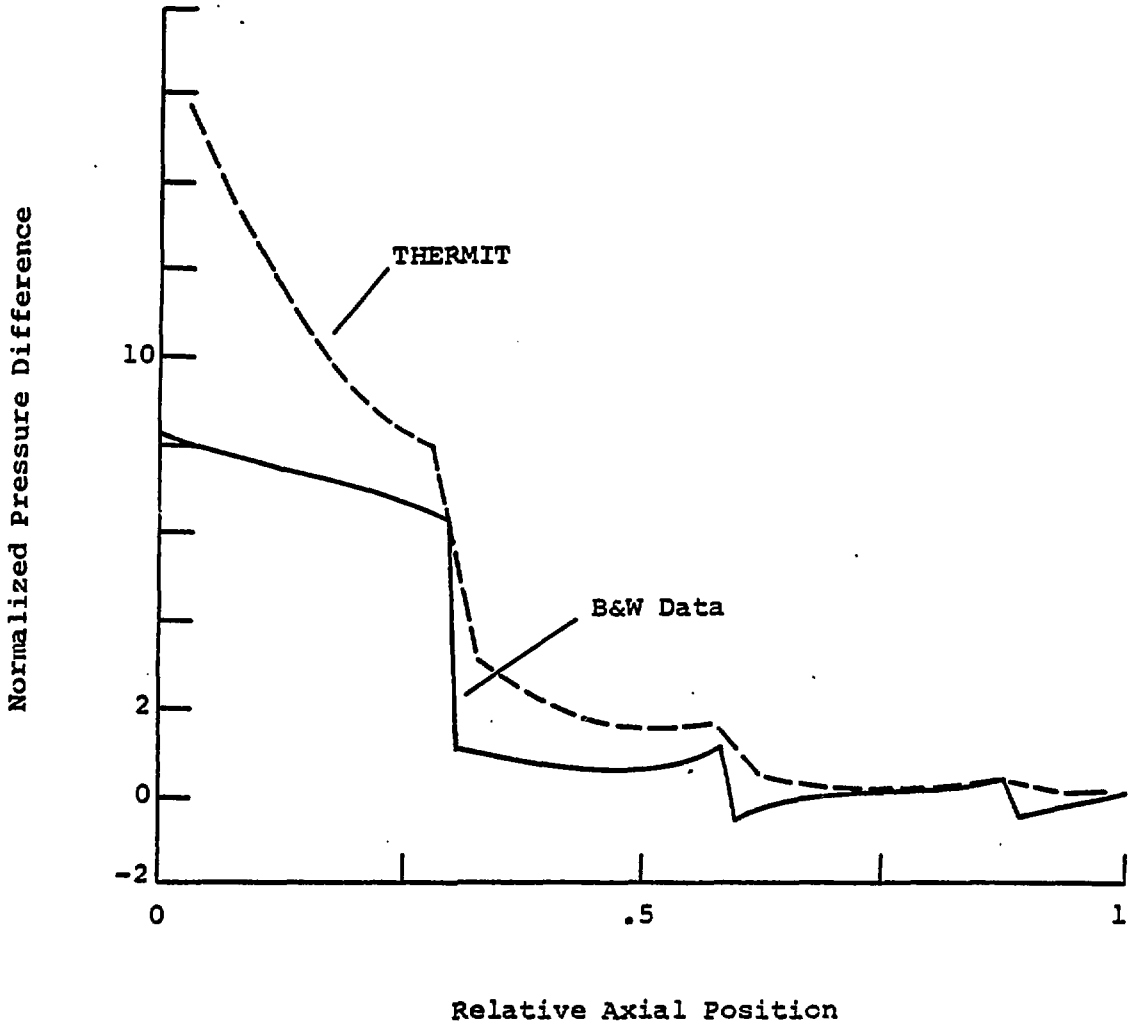

Ref. Stewart, Wolf

Figure 13. Quality Versus Time for Analytic Flow Decay Transient

Figure 14. Local Mass Flow Rate Versus Time for Analytic Flow Decay Transient.

Figure 15. Peak Wall Temperature Versus Time for BWR Rod Drop Accident Model

Figure 16. Peak Wall Temperature Numerical Instability in a Typical PWR Calculation

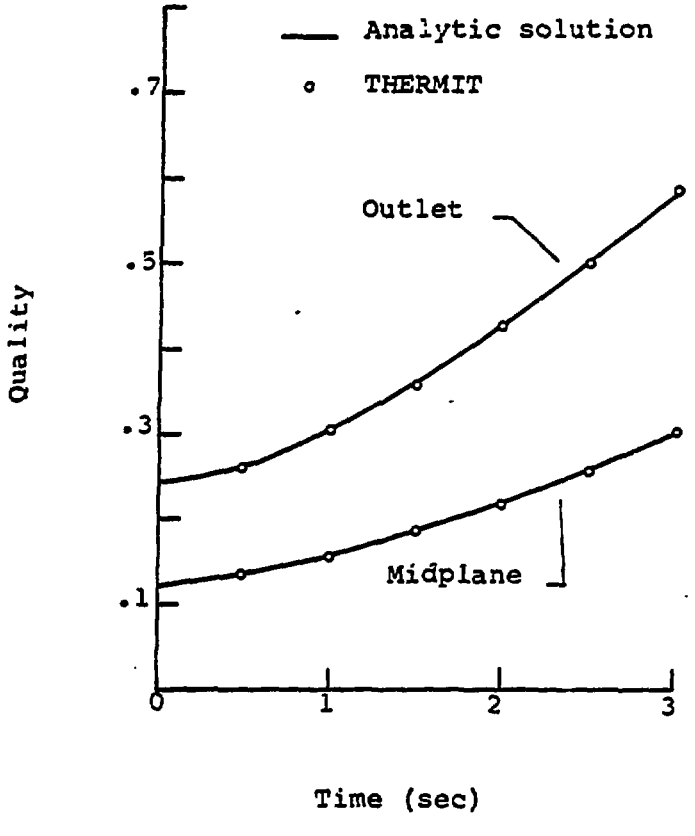
Analytic solution
THERMIT
Outlet
Midplane
Quality
.7
.5
.3
.1
0
1
2
3
Time (sec)

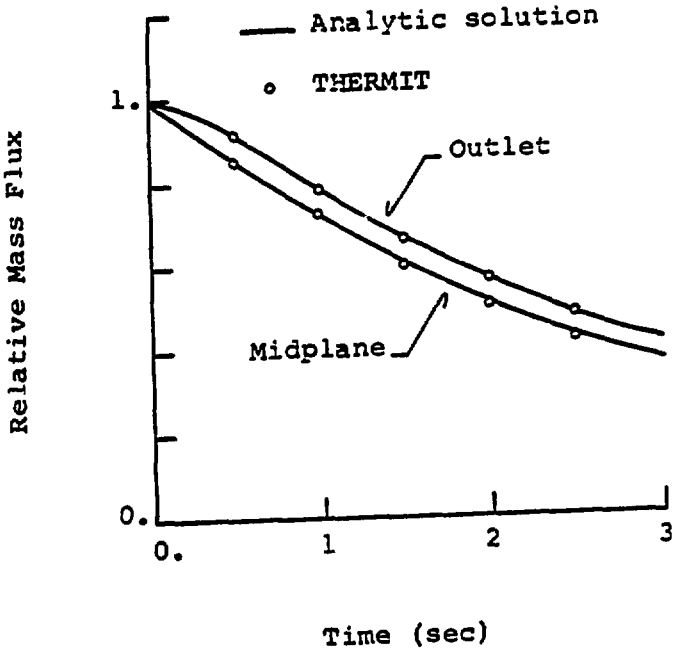
Analytic solution
THERMIT
Outlet
Midplane
Relative Mass Flux
1.
0.
0.
1
2
3
Time (sec)

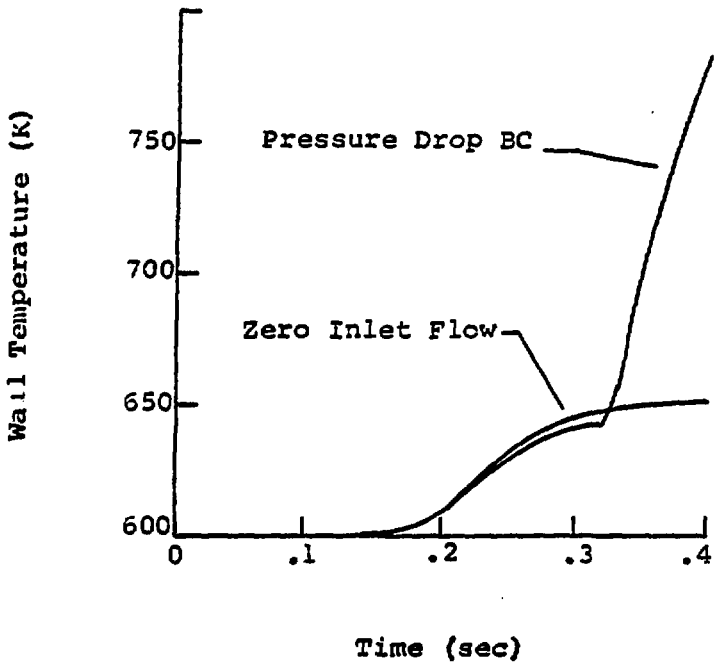
Wall Temperature (K)
750
700
650
600
0
.1
.2
.3
.4
Pressure Drop BC
Zero Inlet Flow
Time (sec)

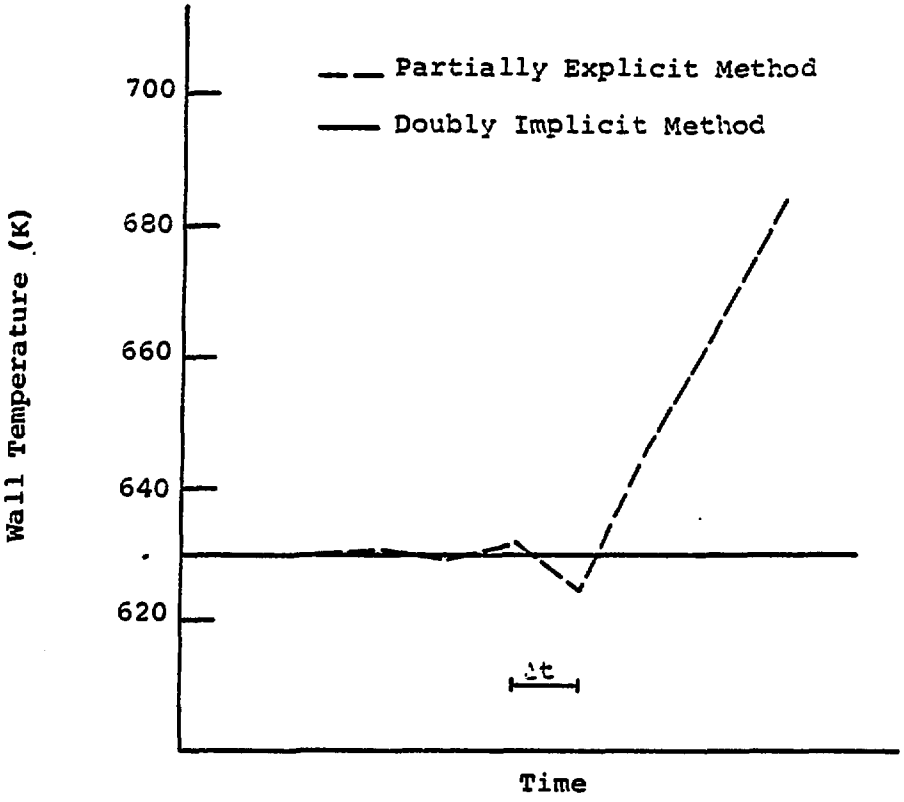
Partially Explicit Method
Doubly Implicit Method
700
680
660
640
620
Wall Temperature (K)
Δt
Time

Figure 17. Comparison of Post-CHF Heat Flux Using Different Numerical Methods

Figure 18. Comparison of Post-CHF Wall Temperatures Using Different Numerical Methods

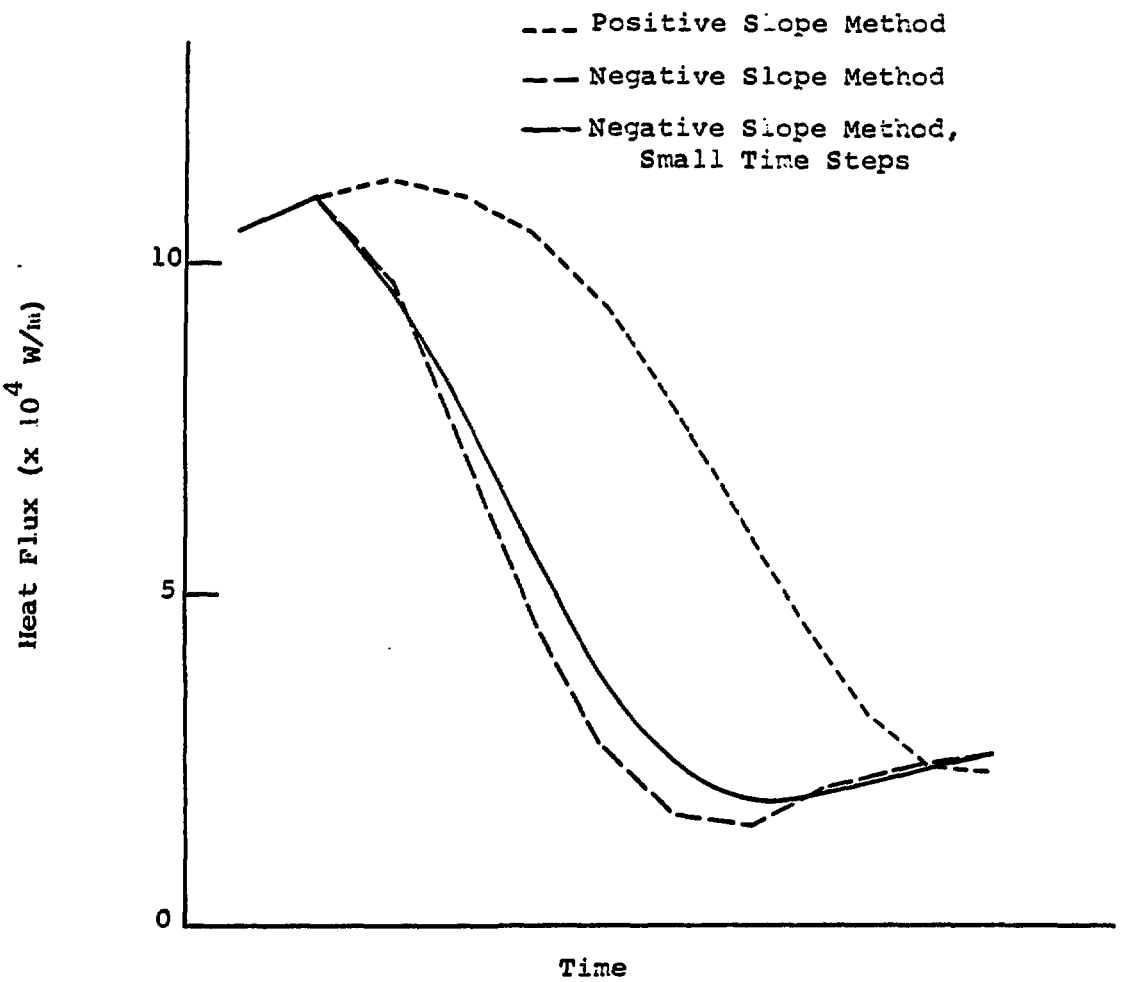
Positive Slope Method
Negative Slope Method
Negative Slope Method, Small Time Steps
Heat Flux (x 10^4 W/m)
10
5
0
Time

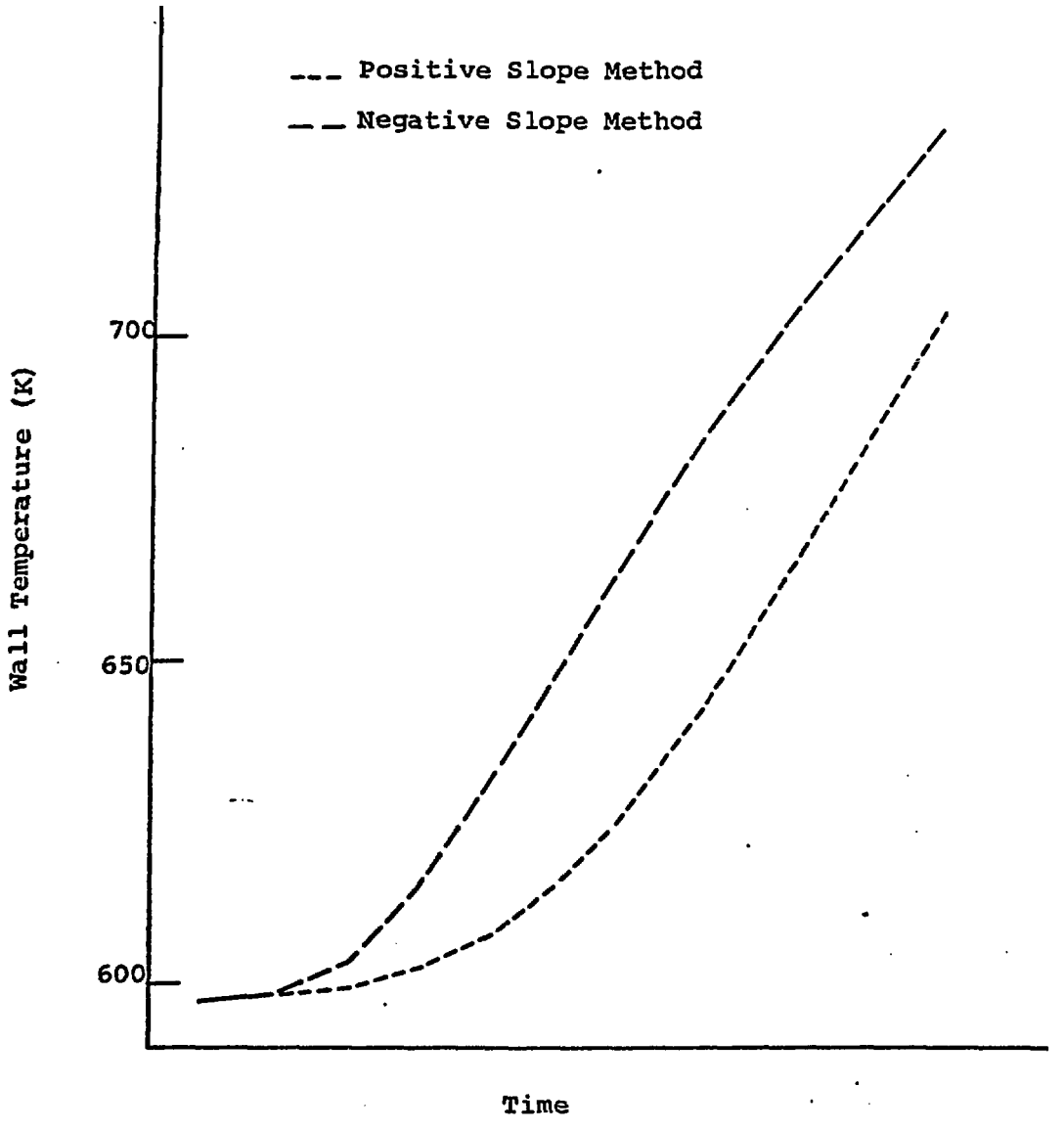

Figure 18

Reed, Stewart, Wolf